Internal magnetic field in $La_{2-x}Sr_xCuO_4$:Gd observed by electron paramagnetic resonance

C. Rettori,* D. Rao, and S. B. Oseroff
Physics Department, San Diego State University, San Diego, California 92182

G. Amoretti
Dipartimento di Fisica, Universita di Parma, I-43100 Parma, Italy

Z. Fisk
Los Alamos National Laboratory, Los Alamos, New Mexico 87545

S-W. Cheong
AT&T Bell Laboratories, Murray Hill, New Jersey 07974

D. Vier and S. Schultz
Physics Department, University of California, San Diego, California 92093

M. Tovar and R. D. Zysler
Centro Atomico Bariloche and Instituto Balseiro, 8400 San Carlos de Bariloche, Rio Negro, Argentina

J. E. Schirber
Sandia National Laboratories, Albuquerque, New Mexico 87185-5800
(Received 27 August 1992)

We have measured the electron paramagnetic resonance (EPR) of Gd^{3+} in single crystals of $La_{2-x}Sr_xCuO_{4+\delta}$, as a function of temperature T, magnetic-field angle, oxygen content, microwave frequency, and Sr concentration ($0 \leq x \leq 0.024$). For temperatures larger than the antiferromagnetic ordering temperature of the Cu lattice, T_N, we have identified four different sites of Gd^{3+} as expected for twinned crystals and we are able to fit the data for all directions of the magnetic field. Samples annealed under vacuum or oxygen show only small changes on their crystal-field parameters and g values. For temperatures smaller than T_N, the EPR lines are further split due to the internal magnetic field acting at the Gd site associated with the antiferromagnetic ordering of the Cu lattice. The temperature dependence of the splitting of the resonance lines allow us to calculate the moment per Cu ion. A value of $\sim 0.6\mu_B$ per Cu ion at $T=0$ K is inferred, with the Cu moments lying in the bc plane about 5° from the c axis. The data only can be fit for all the directions of the applied magnetic field if other mechanisms such as a Heisenberg type of exchange between the Cu and Gd moments or a distortion of the lattice below T_N are included.

I. INTRODUCTION

There have been many suggestions that magnetic interactions play an important role in the high-T_c superconductors.[1,2] A number of experimental studies of the magnetic properties of these materials have been reported in an attempt to clarify the nature of the magnetism of the Cu-O lattice, and its possible relationship to the mechanism of superconductivity.[1,2] These studies include dc and ac magnetization,[3] neutron scattering,[4] μ^+SR,[5] NMR and nuclear quadrupole resonance (NQR),[6] and two-magnon Raman.[7] Many of them have focused on the La_2CuO_4 (T phase) and R_2CuO_4 (R =Pr,Nd,Sm,Eu,Gd) (T' phase) host systems, due to their relatively simple structure. It turns out that these host systems, even without electron or hole dopants, have remarkably complex magnetic features.[3] Despite the difficulties this complexity entails, it is essential to obtain a detailed understanding of all the magnetic properties of these host systems because, once known, even subtle differences in the superconducting versions may prove to be a route to obtain the key insights into the role of magnetism in high-T_c superconductivity. In this paper, we use EPR of dilute local moments, which are placed as probes at the La sites, to clarify the subtle and complex magnetic features of these systems.

Related experiments, in which a local moment (Gd) is substituted for the R-site atom ($R \equiv$Eu), have been reported separately.[8] While there are certain features in common between the La and R hosts, there are also significant differences in the crystal and magnetic structures of these systems which warrant separate consideration and analysis.

We have measured the EPR spectra of Gd^{3+} (doped at 0.1%–1%) in single crystals of $La_{2-x}Sr_xCuO_{4\pm\delta}$, as a function of temperature, T, magnetic-field angle, oxygen content, microwave frequency, and Sr concentration ($0 \leq x \leq 0.024$). We interpret these data and obtain infor-

mation about the magnetic ordering of the Cu-O system and the internal magnetic field acting at the rare-earth site. We determine the crystal-field parameters for the Gd^{3+} ion, and identify the nonequivalent Gd^{3+} sites and their point group symmetry. We also address the problem which arises when working with twinned single crystals and crystals having different oxygen contents.[9]

In Sec. II, the details of sample preparation and experimental techniques are given. In Sec. III, we analyze the point symmetry of the La sites in the La_2CuO_4 crystal structure and present an appropriate spin Hamiltonian for Gd^{3+} ions substituting for La^{3+} ions at the different sites. In Sec. IV, we present our experimental results. In Sec. V, an analysis of the data is given, and in Sec. VI our conclusion are presented.

II. SAMPLE PREPARATION AND EXPERIMENTAL TECHNIQUES

The samples used were single crystal grown in air from CuO-rich flux by slow cooling in Pt crucibles. Their oxygen content has been modified by annealing them under vacuum ($\sim 10^{-6}$ mm) or oxygen pressure (~ 150 atm) at $T \simeq 800$ K. We note that EPR, unlike other techniques, does not require large samples, crystals of 1 mm^3 or less in volume are sufficient. The EPR measurements were made with conventional spectrometers operating at 9 and 35 GHz, at temperatures between 1.5 and 300 K.

III. Gd^{3+} SITE SYMMETRY AND ITS SPIN HAMILTONIAN

At high temperature, the crystals of $La_{2-x}Sr_xCuO_4$ form in a tetragonal phase with $I4/mmm$ symmetry. Each Cu ion is surrounded by an elongated oxygen octahedra and the La ions are surrounded by an array of nine oxygens atoms with a C_{4v} point symmetry. When cooled below ~ 500 K the structure changes to an orthorhombic phase of *Cmca* symmetry with a staggered tilt ($\sim 4°$) of the CuO_6 octahedra, as shown in Fig. 1. In this crystal structure the La ions occupy ($8f$) positions in which their local point symmetry is reduced to C_{1h}. The eight La ions can be grouped into two equivalent sets of four ions that differ only by a translation within the unit cell, and the La ions are still surrounded by nine oxygen neighbors. For Gd^{3+} ions substituting for the La^{3+} ions, an appropriate spin Hamiltonian can be written as[10]

$$H = \mu_B \mathbf{S} \cdot \underline{g} \cdot \mathbf{H} + \sum_{n=2,4,6} \sum_{m=0}^{n} b_n^m O_n^m , \quad (1)$$

where $\underline{g}$ is the giromagnetic-tensor, O_n^m are the Stevens operators, and b_n^m are the corresponding crystal-field parameters (CFP). We have defined a coordinate system in which (x,y,z) are the components of the electron vector position, measured along the a, $-c$, and b crystallographic axes, respectively. The four possible magnetically nonequivalent Gd sites within each unit cell are surrounded by local configurations of atoms differing by a symmetry operation. The spin Hamiltonian for each site can be derived from Eq. (1) by the following transformation in crystal-field terms: (S_x,S_y,S_z) to $(\pm S_x,\pm S_y,\pm S_z)$. The

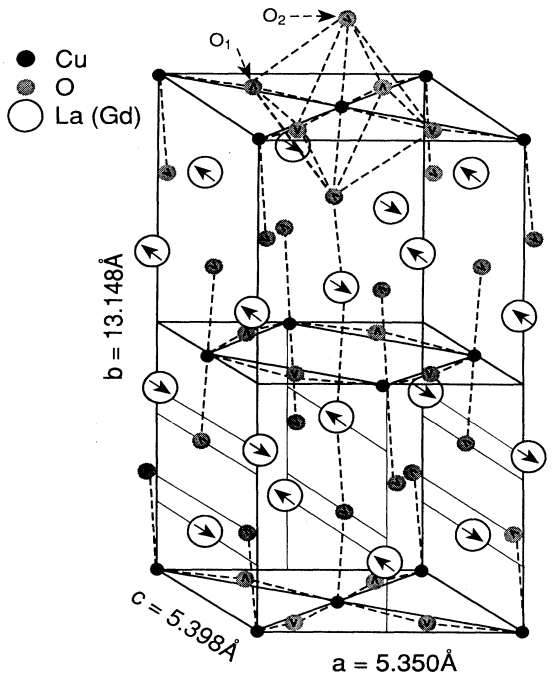

FIG. 1. La_2CuO_4 unit cell showing the eight La atoms which can be grouped into two equivalent sets. Each La(Gd) atom is surrounded by nine nearest oxygen neighbors.

point symmetry C_{1h} (with the reflection symmetry plane being the xz plane) implies that only b_2^0, $b_2^1(s)$, and $b_2^2(c)$ can be different from zero in Eq. (1), corresponding to the operators O_2^0, $O_2^1(s)$, and $O_2^2(c)$. For simplicity we discuss only the terms with $n=2$, a similar analysis applies for $n=4,6$. The eight Gd sites will have the same values of b_2^0 and $b_2^2(c)$ but four will have positive values for $b_2^1(s)$, and the other four have $b_2^1(s)$ negative.

Furthermore, we know that La_2CuO_4 grows as a twinned crystal, that is, with the a axis of the orthorhombic crystal structure being coincident with either the x or the y axis of the reference frame fixed to the macroscopic crystal. The Hamiltonian for the Gd sites in the twinned phase may be obtained by interchanging (S_x,S_y) for $(S_y,-S_x)$ in the crystal-field terms of Eq. (1). Thus, for the other component of the twin phase, b_2^0 remains unchanged, $b_2^2(c)$ changes sign, $b_2^1(s)$ is zero, and $b_2^1(c)$ plays the role of $b_2^1(s)$, changing sign for different Gd sites. As a result we expect four superimposed EPR spectra with the following sets of crystal-field parameters: $[b_2^0,\pm b_2^1(s),b_2^2(c)]$ and $b_2^0,\pm b_2^1(c),-b_2^2(c)$ with $|b_2^1(s)|=|b_2^1(c)|$. The above also apply for the smaller, but non-negligible, terms with $n=4$ and 6.

It has recently been reported that nonstoichiometric superoxygenated $La_2CuO_{4\pm\delta}$ undergoes a phase separation into two closely related orthorhombic phases at a temperature near 270 K.[9] We have not determined the oxygen content of our samples, although the preparation method allows us to estimate that $\delta \leq 0.01$. Samples superoxygenated at 150 bars for two days at 800 K suggest

a phase separation. At room temperature their EPR spectra indicate the presence of a new Gd site. These data will be the subject of a future publication.[11]

The ground state of Gd^{3+} is $^8S_{7/2}$. Thus, each EPR spectrum consists of seven "allowed" fine-structures lines with $\Delta M = \pm 1$ for each site. Since there are four inequivalent sites for a twinned sample, at certain orientations of the applied magnetic field it may be possible to resolve as many as 28 allowed fine-structure lines in the EPR spectrum. Gd^{3+} in La_2CuO_4 has unusually large crystal-field splittings, so the relative intensities of the allowed and the forbidden fine-structure lines are comparable at 9 GHz. With the additional complication of multiple split lines, the analysis of the data is particularly difficult at this frequency. For this reason, most of the data and all of the analysis were performed at 35 GHz, where the relative intensity of the forbidden transitions is diminished.

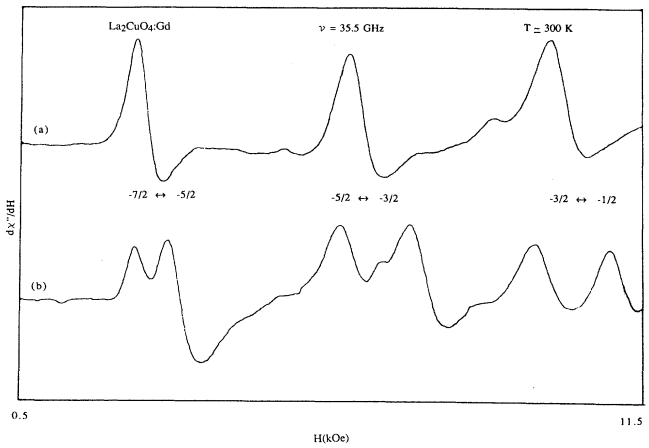

FIG. 3. Low-field La_2CuO_4:Gd EPR spectra at $T = 300$ K ($> T_0$) for (a) $\mathbf{H}_0 \| \mathbf{b}$ axis, (b) $\mathbf{H}_0$ at 25° from the b axis in a plane containing the [101] axis.

IV. EXPERIMENTAL RESULTS

It is well documented that as-grown La_2CuO_4 undergoes an antiferromagnetic transition with a Néel temperature, $T_N \sim 200$–320 K. Below the Néel temperature Yamada *et al.*[4] found that the Cu spins align antiferromagnetically (AF) along the c axis, with a spin canting of $\sim 0.2°$ out of the (a,c) plane. The spin arrangement for the Cu ions is illustrated in Fig. 2. We have found that the Gd^{3+} EPR spectra change at a characteristic temperature T_0 which we identify with T_N. We have studied samples of $La_{2-x}Sr_xCuO_4$, with $x = 0$, 0.009, and 0.024 and find T_0 values of about 250, 200, and 20 K, respectively, which we attribute to the suppression of T_N by the addition of Sr. Measurements of the EPR on single crystals of $La_{0.993}Gd_{0.007}CuO_{4\pm\delta}$ subject to different annealings also have been made. By annealing under vacuum ($\sim 10^{-6}$ mm) for temperatures up to 800–900 K and 48 h, T_0 increased from ~ 250 to ~ 315 K. The value of T_0 is reduced to ~ 195 K when annealed under 150 atm of oxygen at 800 K for 24 h. These values of T_0 are in good agreement with the values of T_N obtained by dc magnetization measurements performed on samples from the same batch. This is consistent with previous studies on the effect of oxygen content on T_N.[9] The EPR spectra obtained above and below T_0 can be summarized as follows.

(a) Paramagnetic region ($T > T_0$). We have found that for $T > T_0$ the EPR spectra can be interpreted as being the result of the superposition of lines from four magnetically nonequivalent Gd^{3+} crystallographic sites for a twinned crystal. At room temperature the individual lines are broad (300–400 G) relative to their spacing and

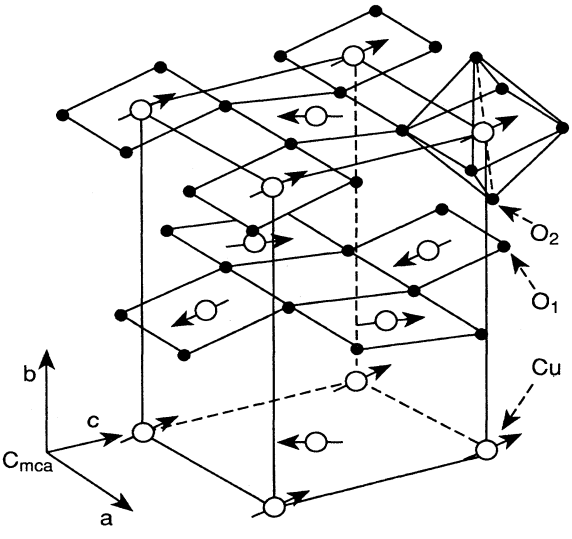

FIG. 2. Orthorhombic structure (space group *Cmca*) of La_2CuO_4. The CuO_6 octahedra are staggered tilt by $\sim 4°$ and the Cu spins canted from the CuO planes by $\sim 0.2°$ according to the neutron data (from Ref. 4).

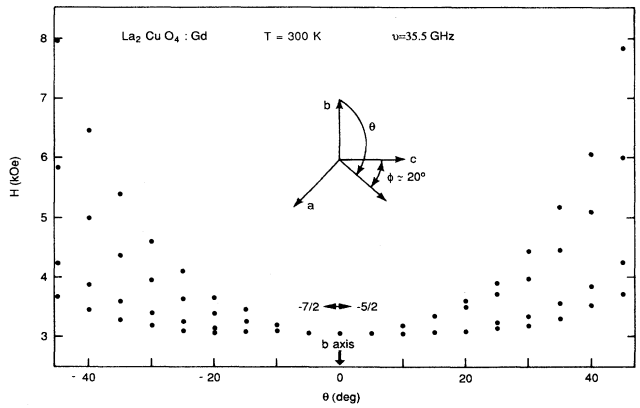

FIG. 4. Angular dependence of the $-\frac{7}{2} \leftrightarrow -\frac{5}{2}$ transition at $T = 300$ K ($> T_0$), when $\mathbf{H}_0$ is rotated from the b axis to an arbitrary plane (see inset).

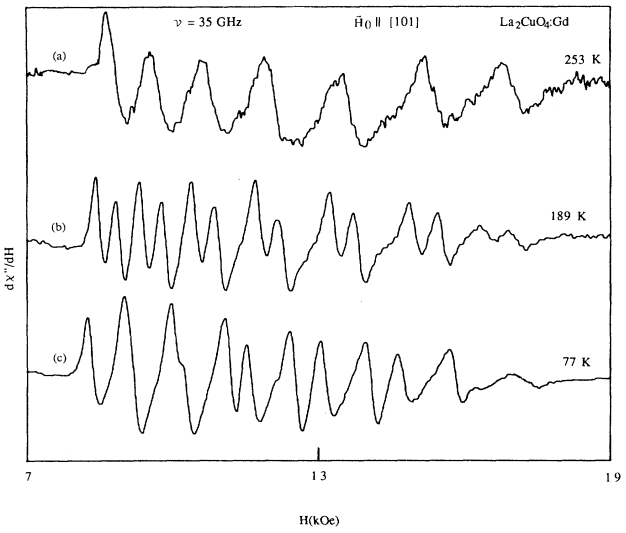

FIG. 5. La_2CuO_4:Gd EPR spectra for $\mathbf{H}_0 \| [101]$ axis at (a) $T \sim 253$ K ($> T_0$), (b) $T \sim 189$ K ($< T_0$), and (c) $T \sim 77$ K ($< T_0$).

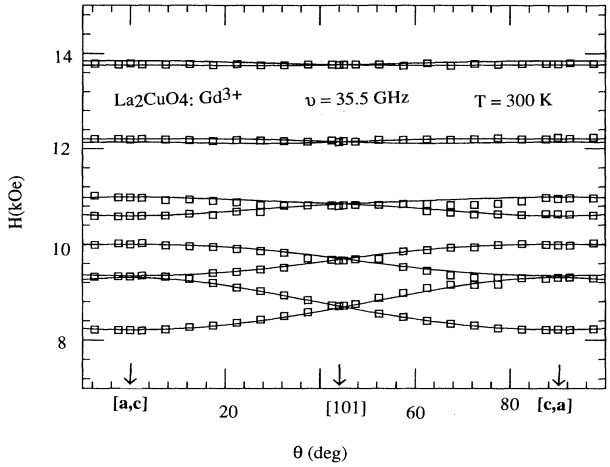

FIG. 7. Angular dependence of the La_2CuO_4:Gd EPR spectra at $T = 300$ K ($> T_0$) for the five lower transitions when $\mathbf{H}_0$ is rotated in the (a,c) plane. The solid lines represent the best fitting of the data obtained by using the parameters listed in Table I.

hence the spectra are only well resolved for certain field orientations. Each of the seven allowed fine-structure lines splits into as many as four components. In particular, when the magnetic field H_0 is applied parallel to the b and [101] axes, the four spectra coalesce into one and each spectral line splits into its four components when H_0 is rotated away from these axes in an arbitrary plane. The four components coalesce into two or three lines when H_0 lies in certain high-symmetry crystallographic planes. In Fig. 3 are shown the spectra with H_0 making angles of 0° and 25° with the b axis and moving in the plane containing the [101] axis (we use the [abc] notation). Notice that each line splits into only two components. In Fig. 4, we present the angular dependence of the $(-\frac{7}{2} \leftrightarrow -\frac{5}{2})$ transition line, showing the full evolution of the fourfold degeneracy when the magnetic field is rotated from the b axis to the (a,c) plane, for the orientation shown in the inset. Because of the complicated spectra, its rapid angular variation, and the considerable linewidth, it is difficult to resolve the individual lines of

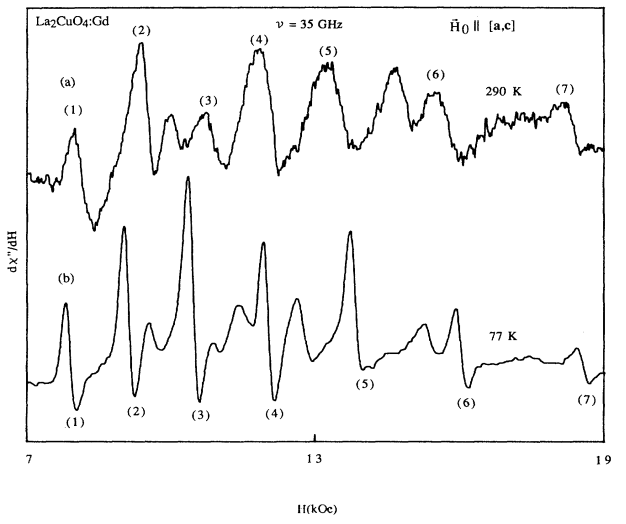

FIG. 6. La_2CuO_4:Gd EPR spectra for $\mathbf{H}_0 \| c$ (or a) axis at (a) $T = 290$ K ($> T_0$) and (b) $T = 77$ K ($< T_0$). The assignments of the resonances corresponding to the fine structure for $\mathbf{H}_0 \| a$ are labeled.

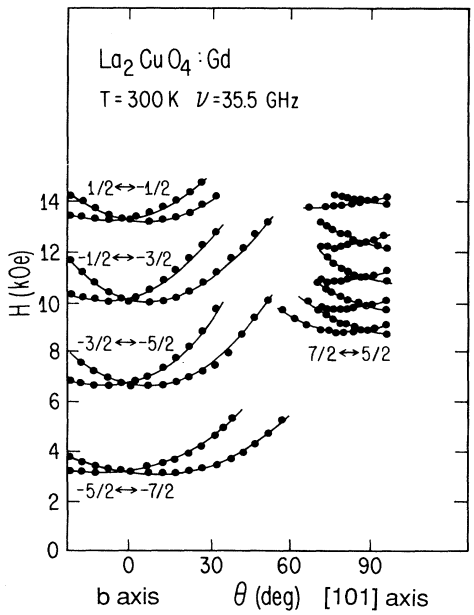

FIG. 8. Angular dependence of the La_2CuO_4:Gd EPR spectra at $T = 300$ K ($> T_0$) for the lower transitions, when $\mathbf{H}_0$ is rotated in the (101) plane.

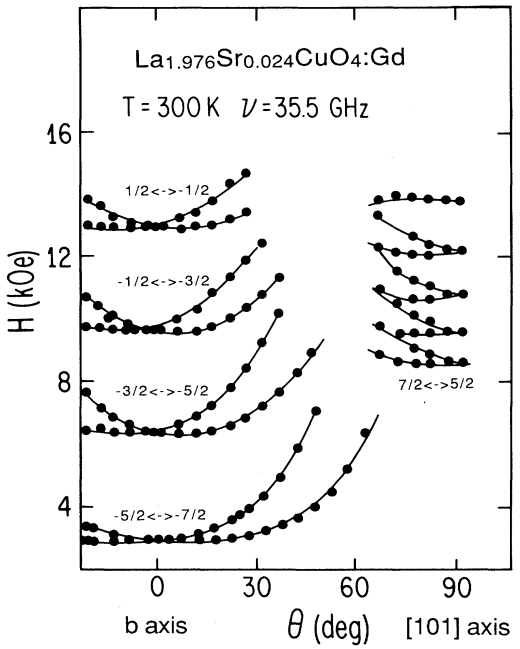

FIG. 9. Angular dependence of the $La_{1.976}Sr_{0.024}CuO_4$:Gd EPR spectra at $T=300$ K ($>T_0$), when $\mathbf{H}_0$ is rotated in the (101) plane.

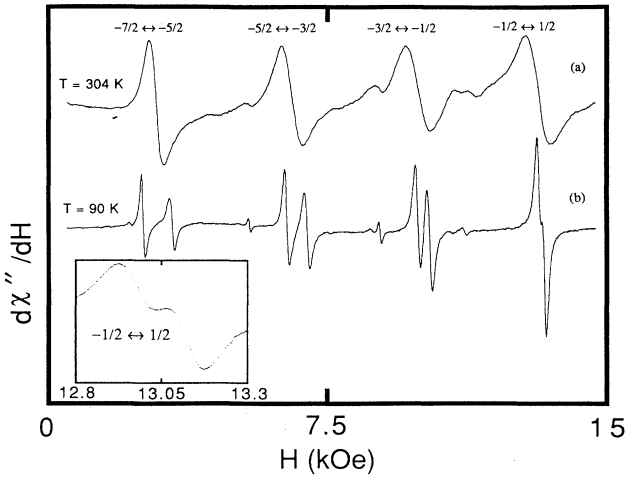

FIG. 11. $La_{1.993}Gd_{0.007}CuO_4$ EPR spectra for the lowest transitions at (a) $T=304$ K ($>T_0$) and (b) $T=90$ K ($<T_0$) for $\mathbf{H}_0\|b$ axis. The inset shows the splitting of the $-\frac{1}{2}\leftrightarrow\frac{1}{2}$ transition. This sample has been superoxygenated at 150 atm and its T_N has been reduced to ~ 190 K.

the other allowed transitions for an arbitrary orientation of the magnetic field. It is also difficult to resolve the spectra when the magnetic field is in the (a,c) plane because the overall splitting is only about half that found when the field is along the b axis. For $\mathbf{H}_0\|[101]$ and $T=253$ K, Fig. 5(a) shows a resolved spectra with the seven fine-structure lines. Figure 6(a) shows a partially resolved spectra for $\mathbf{H}_0\|c$ (or a) and $T=290$ K, note that we are working with twinned crystals. The assignments of the resonances corresponding to the fine structure for $\mathbf{H}\|\mathbf{a}$ are labeled. Figure 7 shows the angular variation in the (a,c) plane at $T=300$ K for the lower transitions. Due to the twinning of our crystals the spectra in this plane appears to have a 90° symmetry.

Data obtained for $La_{2-x}Sr_xCuO_4$:Gd with $x=0.009$ and 0.024 are similar to those found for $x=0$. In Figs. 8 and 9 we present the angular variation of the measured spectra, with $\mathbf{H}_0$ being rotated away from the b axis in the (101) plane, for La_2CuO_4:Gd and $La_{1.976}Sr_{0.024}CuO_4$:Gd, respectively. As in Fig. 3, the data for this orientation of the field show the Gd sites grouped into two lines.

(b) Antiferromagnetic region ($T<T_0$). As we lower the temperature below ~ 250, 200, or 20 K for $x=0$,

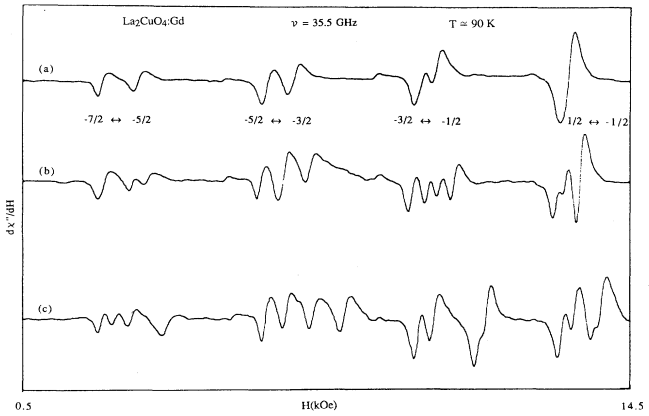

FIG. 10. $La_{1.993}Gd_{0.007}CuO_4$ EPR spectra at $T=90$ K ($<T_0$) when $\mathbf{H}_0$ is rotated in a plane containing the b and [101] axes, (a) $\mathbf{H}_0$ along the b axis, (b) $\mathbf{H}_0$ at 10° from the b axis, and (c) $\mathbf{H}_0$ at 20° from the b axis.

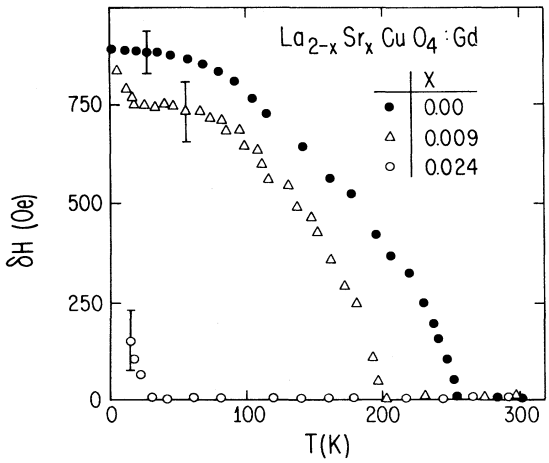

FIG. 12. Temperature dependence of the splitting δH of the $-\frac{7}{2}\leftrightarrow-\frac{5}{2}$ transition for $\mathbf{H}_0\|b$ in $La_{2-x}Sr_xCuO_4$:Gd ($x=0$, 0.009, and 0.024). Notice the sharp increase in δH for $x=0.009$ at ~ 20 K.

0.009, and 0.024, respectively, each of the EPR lines observed for $T > T_0$ are further split. A similar behavior is observed for the annealed samples of La_2CuO_4:Gd, where the extra splitting occurs at a temperature near the value of T_N measured by dc magnetization. Fortunately the linewidths decrease, so we are able to resolve the spectra despite the added complexity. This further splitting is basically independent of the microwave frequency used (9 and 35 GHz) and increases as the temperature is lowered. In Fig. 10, we show the spectra for $La_{1.993}Gd_{0.007}CuO_4$ measured at $T \sim 90$ K, $\nu = 35.5$ GHz, with $\mathbf{H}_0$ making angles of 0°, 10°, and 20° with the b axis, and moving in the plane containing the [101] axis. Here, each of the lines that was observed above T_0 is further split into two components. Note that this splitting even occurs for 0°, i.e., with $\mathbf{H}_0$ along the b axis. Figure 11 shows these splittings

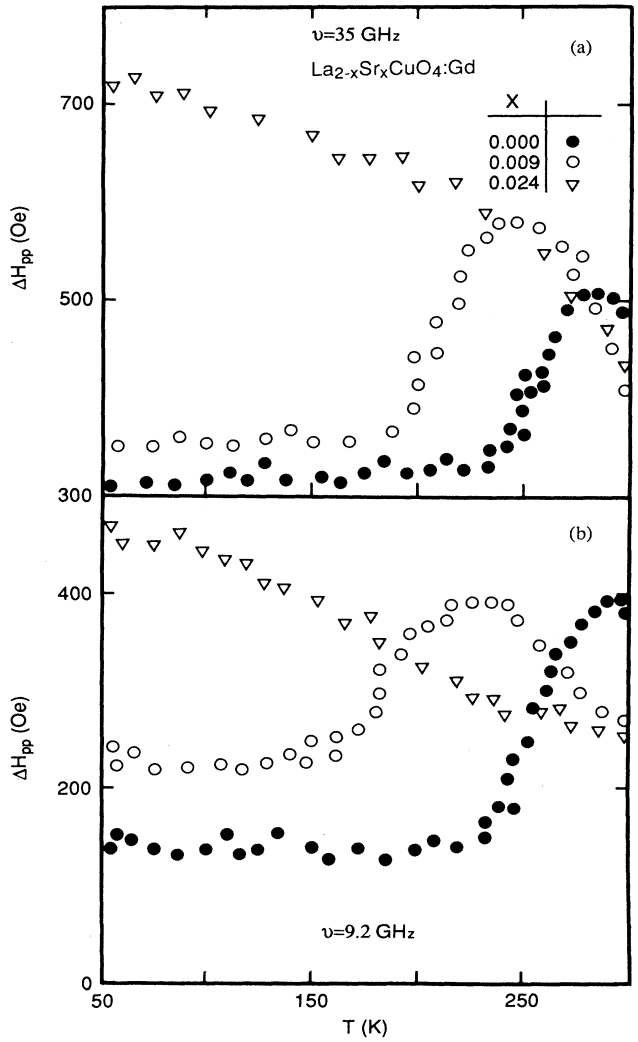

FIG. 13. Temperature dependence of the linewidth ΔH_{pp} for $\mathbf{H}_0 \| b$ in $La_{2-x}Sr_xCuO_4$:Gd ($x = 0$, 0.009, and 0.024) (a) $-\frac{7}{2} \leftrightarrow -\frac{5}{2}$ transition at 35 GHz and (b) $-\frac{3}{2} \leftrightarrow -\frac{1}{2}$ transition at 9.2 GHz.

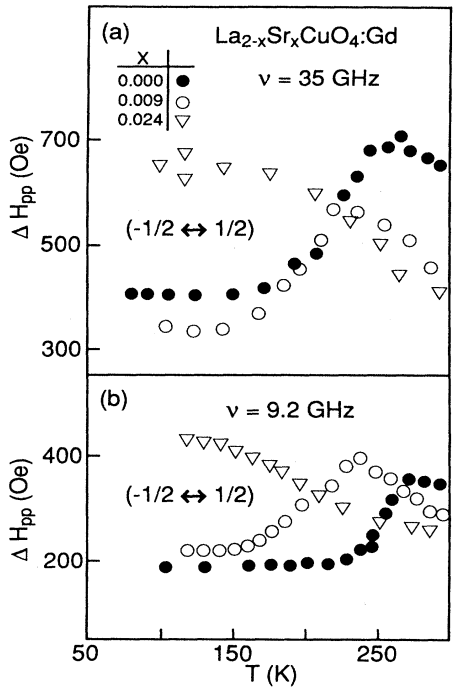

FIG. 14. Temperature dependence of the linewidth ΔH_{pp} for the $-\frac{1}{2} \leftrightarrow \frac{1}{2}$ transition and $\mathbf{H}_0 \| b$ in $La_{2-x}Sr_xCuO_4$:Gd ($x = 0$, 0.009, and 0.024), (a) 35 GHz and (b) 9.2 GHz.

for a superoxygenated sample of La_2CuO_4:Gd with $T_N \sim 190$ K; the inset shows the splitting for the $-\frac{1}{2} \leftrightarrow \frac{1}{2}$ transition for $T = 90$ K.

In Fig. 12, we present δH, the splitting of the $-\frac{7}{2} \leftrightarrow -\frac{5}{2}$ line, as a function of temperature for $\mathbf{H}_0$ parallel to the b axis and $x = 0$, 0.009, and 0.024. In Fig. 13,

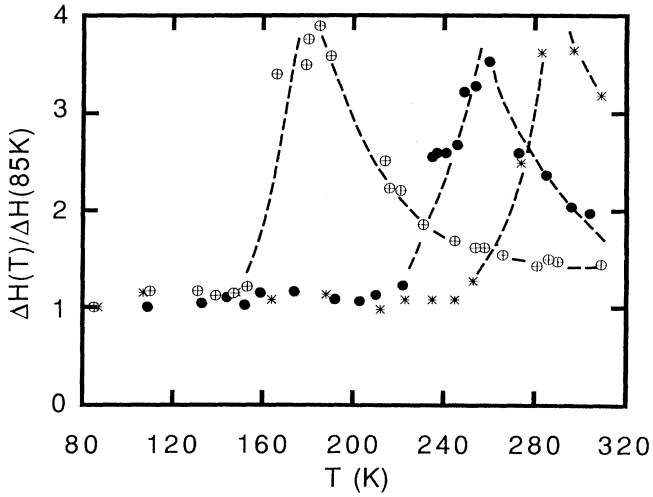

FIG. 15. Normalized linewidth for the $-\frac{7}{2} \leftrightarrow -\frac{5}{2}$ transition as a function of temperature for a single crystal of $La_2CuO_{4+\delta}$:Gd at 35.5 GHz and $\mathbf{H}_0 \| \mathbf{b}$, (●) as-grown $T \sim 250$ K; (*) vacuum annealed at 800 K for 4 h, $T_N \sim 300$ K; (⊕) superoxygenated at 150 bars for 2 days at 800 K, $T_N \sim 190$ K. The solid lines is a guide for the eye.

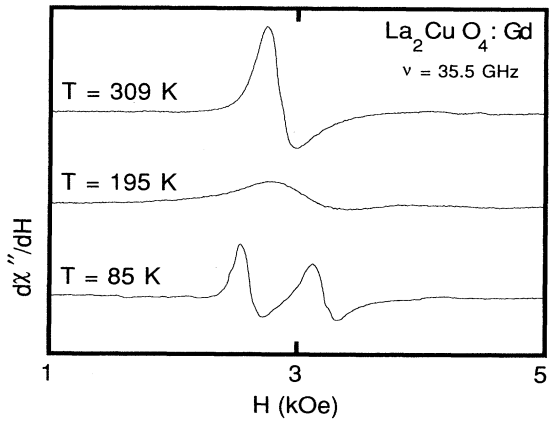

FIG. 16. La_2CuO_4:Gd EPR spectra for the $-\frac{7}{2}\leftrightarrow-\frac{5}{2}$ transition in a superoxygenated sample, $T_N\sim 190$ K, taken at different temperatures.

we show the linewidths of the $-\frac{3}{2}\leftrightarrow-\frac{1}{2}$ and the $-\frac{7}{2}\leftrightarrow-\frac{5}{2}$ transitions with $\mathbf{H}_0$ parallel to the b axis, as a function of temperature for $x=0$, 0.009, and 0.024 and for $\nu=9.2$ and 35.5 GHz, respectively. Figure 14 shows, for the same samples and frequencies, the temperature dependence of the linewidth of the $-\frac{1}{2}\leftrightarrow\frac{1}{2}$ transition, with $\mathbf{H}_0\|\mathbf{b}$. Figure 15 shows the normalized linewidth for the $-\frac{7}{2}\leftrightarrow-\frac{5}{2}$ transition as a function of temperature with $\mathbf{H}_0\|\mathbf{b}$ for a single crystal of $La_2CuO_{4\pm\delta}$ subject to different annealings. The crystal as grown shows a maximum in ΔH_{pp} at ~ 260 K, after vacuum annealing the temperature of the maximum increases to ~ 300 K and when superoxygenated at ~ 150 bars it decreases to ~ 190 K. At low temperatures, when the splittings are well resolved, the plotted linewidth in Figs. 13–15 corresponds to that of a single line, whereas at higher temperatures, when the splittings are unresolved, the composite

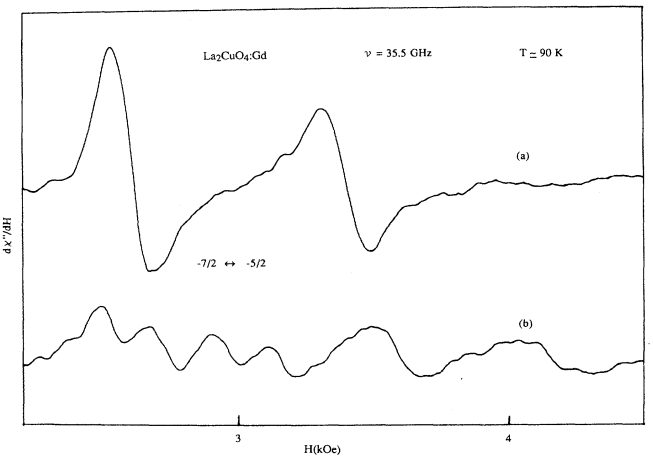

FIG. 17. La_2CuO_4:Gd $-\frac{7}{2}\leftrightarrow-\frac{5}{2}$ transition at $T=90$ K ($<T_0$) when $\mathbf{H}_0$ is rotated in a plane containing the v axis and the a or c axis (a) $\mathbf{H}_0$ along the b axis and (b) $\mathbf{H}_0$ 25° from the b axis.

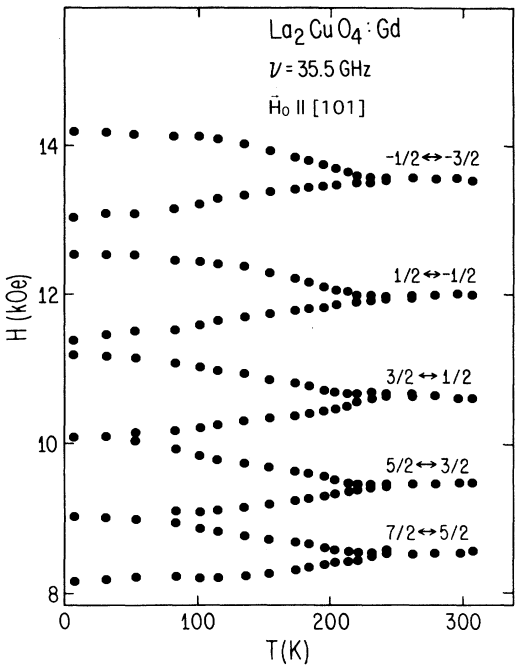

FIG. 18. Temperature dependence of the splitting for the various transitions for $\mathbf{H}_0\|[101]$ axis.

width is plotted. This is illustrated in Fig. 16 for the superoxygenated sample of Fig. 15.

The EPR spectra for the transition $-\frac{7}{2}\leftrightarrow-\frac{5}{2}$, for $x=0$, $T=90$ K, $\nu=35.5$ GHz, and for $\mathbf{H}_0$ making angles of 0° and 25° with the b axis in the plane containing the a or c axis, are shown in Figs. 17(a) and 17(b), respectively. For the latter, note that the three lines observed above T_0 have split into six lines.

In (a) we presented Fig. 5(a) to illustrate the EPR spectra for $La_{1.993}Gd_{0.007}CuO_4$ with $\mathbf{H}_0$ parallel to [101], mea-

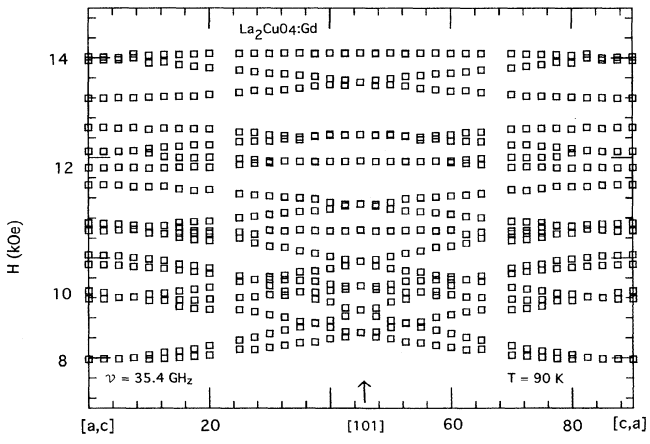

FIG. 19. Angular dependence of the La_2CuO_4:Gd EPR spectra for the five lowest transitions measured at $T=90$ K ($<T_0$) and $\nu=35.4$ GHz, when $\mathbf{H}_0$ is rotated in the (a,c) plane. Notice that the data correspond to a twinned crystal.

sured at 35.02 GHz for $T=253$ K, i.e., $T>T_0$. As mentioned there, the spectra for the four nonequivalent Gd^{3+} sites coalesce, and only the seven allowed fine-structure lines are observed. As we lower the temperature each of these lines splits into two components, as is shown in Fig. 5(b) for $T=189$ K. As the temperature is lowered further, the splitting increases, and the different components start to overlap, as is shown in Fig. 5(c) for $T=77$ K. The splitting of a given transition with $\mathbf{H}_0\|[101]$ into its pair of components as a function of temperature between 4 and 300 K is shown in Fig. 18. In Fig. 6, the EPR spectra for $\mathbf{H}_0$ parallel to the a or c axis are shown for 290 and 77 K. The assignments of the resonances corresponding to the fine structure for $\mathbf{H}_0\|\mathbf{a}$ are given. For $T<T_0$ it is difficult to identify the lines for $\mathbf{H}_0\|\mathbf{c}$ because of our twinned crystals and also because, for this orientation, the line separations due to the crystal field are relatively small and the splittings of the lines are large. This is illustrated in Fig. 19 where the angular variation for the five lower transitions in the (a,c) plane at $T=90$ K is plotted for a superoxygenated crystal with $T_N\sim190$ K. For convenience, the data in the (a,c) plane were taken in a crystal with T_N (~190 K) such that the overlapping of the different split lines is minimized at a temperature easy to stabilize in our experimental setup. That temperature in our case was $T\simeq90$ K. Splitting of lines which are temperature dependent, like those shown in Fig. 18, were also measured for $\mathbf{H}_0\|\mathbf{a}$ (or $\mathbf{c}$), but with a more complicated spectra because of the reasons given above.

V. DATA ANALYSIS AND DISCUSSION

Our goals are to interpret the measurements presented in Sec. IV to characterize the nature of different Gd^{3+} sites, to determine g values, crystal-field parameters, and to obtain information about the magnetic ordering of the Cu-O planes. As there are qualitative differences between the spectra obtained above and below T_0, we again discuss the two temperature regimes separately.

A. Analysis for $T>T_0$

The analysis presented here is restricted to the data taken at $\nu\sim35$ GHz and for $x=0$. Other than the reduction in T_0 there were no substantive differences in the data taken for samples with $x\neq0$. We found that the set of crystal-field parameters for $x=0$ holds reasonably well for the samples with $x=0.009$ and 0.024, as well as for the samples annealed under vacuum or excess of oxygen.

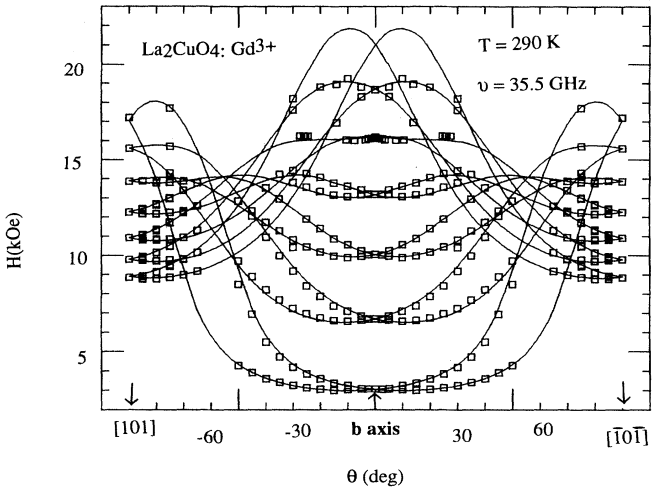

FIG. 20. Best fitting for the data taken in the $(b,[101])$ plane at 290 K using the parameters listed in Table I.

The complicated spectra obtained for an arbitrary orientation of the external magnetic field are simplified, when observed along the a, b, c, and [101] directions [see Figs. 3(a), 5(a), 6(a), and 11(a)]. By assuming that the spectra comes from two magnetically nonequivalent Gd^{3+} sites in the unit cell, and taking into consideration the twinning of the crystals, we were able, using the Hamiltonian of Eq. (1), to fit, better than within half a linewidth, the field for resonance for the allowed transitions observed along all the directions. The best fit of the experimental data yields the g values and crystal-field parameters listed in Table I. Using these parameters and Eq. (1) we have simulated the theoretical angular variation expected for the spectra in different planes. We show the simulation for the $(b,[101])$ plane (see Fig. 20) and in the (a,c) plane (see Fig. 7). For simplicity, only part of the experimental data have been included in these two figures. The theoretical curves and the experimental data are in very good agreement.

In summary, the g values and CFP given in Table I applied to the four sites present in a twinned crystal predict a coincident overlapping of the spectra for $\mathbf{H}_0$ parallel to the b axis, the splitting of each line into two lines when $\mathbf{H}_0$ is rotated toward the [101] axis, into three when mov-

TABLE I. g values and crystal-field parameters at 290 K for a sample of La_2CuO_4:Gd^{3+} as grown with $T_N\sim250$ K.

g values	b_2^m (10^{-4} cm^{-1})	b_4^m (10^{-4} cm^{-1})	b_6^m (10^{-4} cm^{-1})
$g_x=1.977\pm0.001$	$b_2^0=-1378\pm5$	$b_4^0=-4\pm1$	$b_6^0=-3\pm1$
$g_y=1.974\pm0.001$	$b_2^1=-2013\pm10$	$b_4^1=-55\pm10$	$b_6^1=80\pm10$
$g_z=1.970\pm0.001$	$b_2^2=-238\pm5$	$b_4^2=-3\pm2$	$b_6^2=15\pm10$
		$b_4^3=-10\pm5$	$b_6^3=-50\pm10$
		$b_4^4=10\pm5$	$b_6^4=-10\pm10$
			$b_6^5=160\pm20$
			$b_6^6=10\pm5$

ing toward the a or c axis, and into four when rotated to any other axis in the plane. All this is in agreement with the experimental data.

B. Analysis for $T < T_0$

Dramatic changes in the EPR spectra are observed for $T < T_0$. The changes are similar for $x = 0$, 0.009, and 0.024, and for the samples as grown they are first observed at ~ 250, 200, and 20 K, respectively, corresponding approximately to their Néel temperatures.

It is possible to explain the data below T_0 by adding to the spin Hamiltonian of Eq. (1) a pseudo-Zeeman energy term associated with an internal magnetic field H_i, lying approximately in the (a,c) plane. The fact that the splitting appears at $T_0 \simeq T_N$ strongly suggests that the origin of this internal field is associated with the magnetic ordering of the Cu moments. As seen in Fig. 2, below T_N the La (Gd) sites in adjacent unit cells are surrounded by reverse configurations of Cu moments. These spin arrangements create two different La (Gd) sites in the magnetic structure with equal probability of occurrence. The two different La (Gd) sites "see" an internal field H_i of the same magnitude but different sign. We calculate the internal field at the La (Gd) site which arises from the dipolar field of the AF ordered Cu moments. By adding up the contribution of the dipoles around the La (Gd) site from a sphere of 400 A, we have calculated the dipolar field using the magnetic structure proposed by neutron scattering[4] and μ^+SR (Ref. 5) experiments. The measured internal field inferred from our experiments correspond to $\sim 0.6\mu_B$ per Cu ion at 4 K, in good agreement with the value deduced from previous measurements.[4,5] The g values, CFP, and H_i for the best fit of the data at 90 K are given in Table II. The best fit of the data is obtained with H_i lying in the (b,c) plane, making an angle of $\sim 5°$ with the c axis. In Fig. 21, we present the fitting for the $(b,[101])$ plane using the parameters listed in Table II. In Fig. 22, we show the best fit to the data taken at 90 K in the (a,c) plane for a superoxygenated sample with $T_N \sim 190$ K. In that case we use the g values and CFP listed in Table II, but a value of $H_i = 385$ Oe was used instead of 650 Oe. The difference in H_i is because T_N for that sample has been reduced from ~ 250 to ~ 190 K by annealing it in 150 atm of oxygen. In Figs. 21 and 22, for simplicity, we have included just the data corresponding to only one of the twins, simulating the

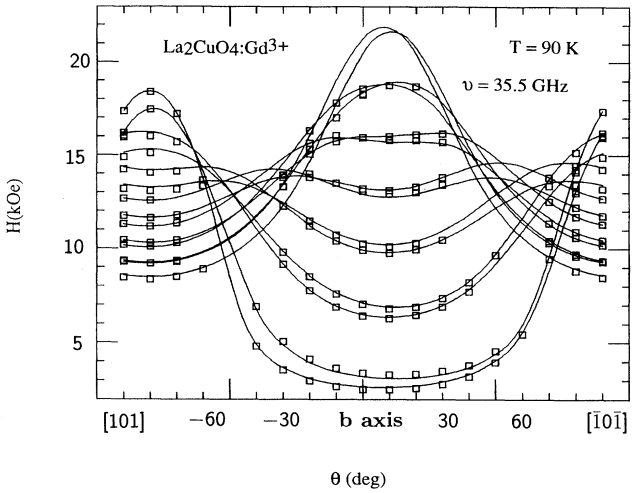

FIG. 21. Best fitting for the data taken in the $(b,[101])$ plane at 90 K and 35.5 GHz using the parameters listed in Table II. We have included only the data corresponding to one of the twins.

data of an "untwinned" single crystal. The average splitting for the different transitions in the (a,c) plane at 90 K for the sample illustrated in Fig. 22 is shown in Fig. 23 as a function of angle. The solid line corresponds to $\delta H = 2H_i \sin\theta(\text{Oe}) = 770 \sin\theta(\text{Oe})$.

The agreement between the data and the simulation is very good in almost all the cases, however, as can be seen in Fig. 21 for the applied magnetic field H making angles of $\sim 30°$ or less with the b axis, the data for the lowest transitions cannot be fit within the experimental error. The origin of these differences may result from one of the following mechanisms not considered in our model: (i) A Heisenberg type of exchange between the Gd ions and the Cu moments, of the form $\sum_k J_k S_{\text{Gd}} S_{\text{Cu}}^{(k)}$. Its contribution to the internal field will depend on the local canting of the Cu moments and, in principle, it will not point in opposite directions for neighboring Gd sites. If so, the internal fields acting on neighboring Gd ions may differ in magnitude and not be perfectly antiparallel, as is the case when they are due only to the dipolar field of the Cu moments. If we allow the internal fields "seen" by the Gd sites to differ $\sim 10\%$ in magnitude and $\sim 10°$ from being

TABLE II. g values, crystal-field parameters and internal magnetic field at 90 K for $La_2CuO_4:Gd^{3+}$ as grown with $T_N \sim 250$ K.

g values	b_2^m (10^{-4} cm^{-1})	b_4^m (10^{-4} cm^{-1})	b_6^m (10^{-4} cm^{-1})	H_i (Oe)
$g_x = 1.976 \pm 0.001$	$b_2^0 = -1366 \pm 10$	$b_4^0 = -12 \pm 1$	$b_6^0 = -1 \pm 1$	650 ± 30
$g_y = 1.981 \pm 0.001$	$b_2^1 = -2040 \pm 10$	$b_4^1 = -70 \pm 10$	$b_6^1 = 50 \pm 10$	
$g_z = 1.982 \pm 0.001$	$b_2^2 = -335 \pm 5$	$b_4^2 = -4 \pm 2$	$b_6^2 = 15 \pm 10$	
		$b_4^3 = 140 \pm 20$	$b_6^3 = 3 \pm 3$	
		$b_4^4 = 25 \pm 5$	$b_6^4 = -10 \pm 10$	
			$b_6^5 = 150 \pm 20$	
			$b_6^6 = 10 \pm 5$	

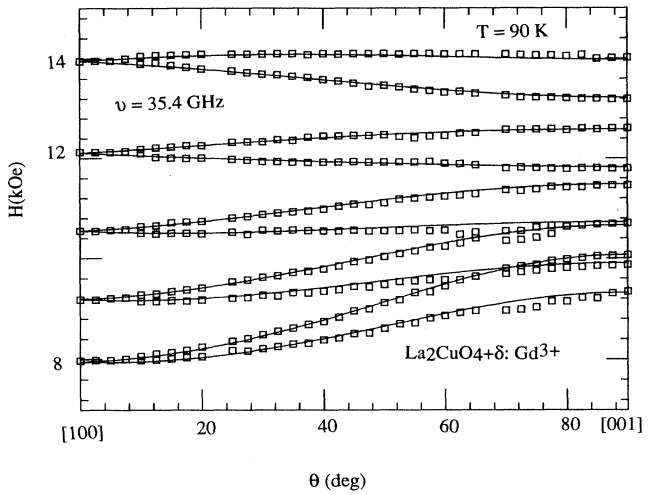

FIG. 22. Best fitting to the data taken at 90 K and 35.4 GHz, when $\mathbf{H}_0$ is rotated in the (a,c) plane, using the parameters listed in Table II, but with $H_i = 385$ Oe (see text). For clarity we have used the data corresponding to only one of the twins.

perfectly antiparallel, then the data can be fit for all directions and temperatures within the experimental error. (ii) Another way to explain the observed differences is that the AF ordering in conjunction with the spin canting of the Cu moments may produce shifts in the ionic coordinates within each unit cell and give rise to an internal magnetostriction. Furthermore, the induced ionic displacements within the unit cell could result in changes of the crystal electric field and orbital overlaps. Such changes may give rise to shifts in the position of the fine-structure lines of Gd^{3+}, which could also lower the symmetry of the spin site. However, the symmetry at the Gd^{3+} site is already low, C_{1h}, so we expect to observe

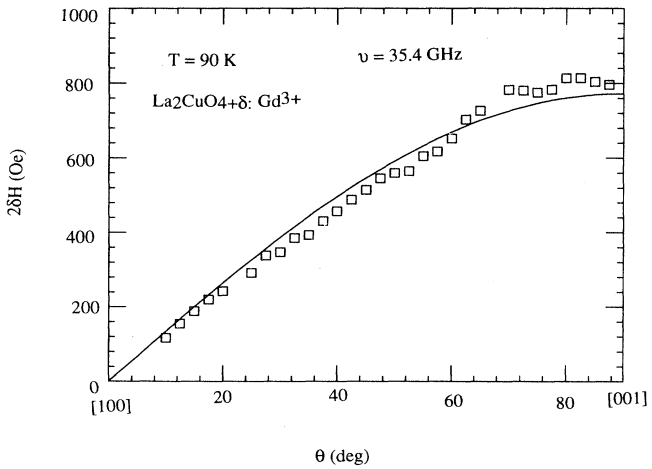

FIG. 23. The angular dependence of the average splitting for the different transitions in the (a,c) plane at 90 K for the twin illustrated in Fig. 22. The solid line is the fitting with $\delta H = 770x \sin\theta$ Oe, with $\theta = 0°$ for $H \| [100]$ and $\theta = 90°$ for $H \| [001]$ (see text).

changes mainly in the magnitude of the crystal-field parameters. We can improve the fitting of the data if we assign a different set of CFP's to each of the Gd sites created below T_0, keeping an internal magnetic field of the same magnitude and different sign acting on each of them. A different set of CFP's, below T_0, for each Gd site may result from an induced internal ionic displacement, if half of the Gd sites sees an expansion, and the other half a contraction of their unit cell, or an equivalent half sees a reduction and the other half an increase of their CFP's. It is interesting to note that below T_0 and with H making an angle of $\lesssim 30°$ with the b axis, the linewidth of the split lines associated with a given transition [see Figs. 10(a), 15(a), and 16(a)] supports a larger distribution of resonance field, that is, larger linewidths, for those sites "having the smaller CFP."

The dependence of δH on the Sr concentration, x, is similar to that found by NQR by Watanabe *et al.*[6] for the ordering of $La_{2-x}Ba_xCuO_4$ including the abrupt change observed at ~ 20 K for $x = 0.009$. These authors argued that a possible origin of the increase in the internal field at low temperature may be due to a change from incoherent ordered state to a coherent one.

The large broadening of the linewidths at $T \gtrsim T_0$ shown in Figs. 13–16 is observed in all the samples studied. Its origin is possible due to slow magnetic fluctuations present at $T > T_0$.

VI. CONCLUSIONS

For $T > T_0$ we have identified four different sites of Gd^{3+} in $La_{2-x}Sr_xCuO_4$, each with C_{1h} local point symmetry. The number of nonequivalent Gd^{3+} observed is that expected for twinned crystals. The crystal-field parameters listed in Table I fit the data within the experimental error, for all the directions of the magnetic field. Samples annealed under vacuum or oxygen, as the one doped with Sr up to $x = 0.024$, show only small changes on their CFP's from the values listed in Table I.

For $T < T_0$ further splittings of the EPR lines are found. The values of T_0 are in good agreement with the values of T_N determined by dc magnetization for the samples of $La_{2-x}Sr_xCuO_4$, $x = 0$, 0.009, and 0.024, as for the samples of La_2CuO_4 annealed under vacuum or oxygen. The changes in the EPR spectra found at $T < T_0$ are associated with the magnetic ordering of the Cu lattice. Several signatures in the EPR spectra that result from this magnetic ordering are observed. One is the presence of an internal field at the Gd site whose origin, at least most of it, is due to the dipolar field associated to the AF ordered Cu moments. The temperature dependence and magnitude of the splitting of the lines implies $\sim 0.6\mu_B$ per Cu ion at $T = 0$ K, for a magnetic structure with the Cu moments lying in the (b,c) plane about 5° from the c axis, which is in good agreement with the magnetic structure suggested by neutron experiments.[4]

The data below T_0 can be fitted within the experimental error for all the directions of the applied magnetic field, but for H lying within $\sim 30°$ of the b axis. In that case, the difference between the fitting and the data is

about twice the experimental error. It is possible that other mechanisms, such as a Heisenberg type of exchange interacting between the Cu and Gd moment, or a distortion of the lattice below T_0 due to the AF ordering of the Cu moments can be the origin of the differences found. In fact, we can fit the data within the experimental error, if we allow for an extra contribution to the internal field such that neighboring Gd ions are subject to internal magnetic fields $\sim 10\%$ different in magnitude and not exactly antiparallel. We also can fit the data within the experimental error keeping an internal field of the same magnitude and different sign acting on neighboring Gd sites, but allowing for different CFP's for each of the Gd sites.

Another interesting feature observed at both frequencies for the samples studied is a well-defined maximum in the linewidth at $\sim T_0$ for all the transitions and orientations. Its origin is possible due to slow magnetic fluctuations present above the temperature at which a three-dimensional ordering occurs. Finally, it should be mentioned that because our EPR data are observed in a "foreign" species (Gd^{3+}) substituting for La^{3+} ions, the interpretation of our data should be taken with some reservations.

In summary, our data show that in spite of the difficulties in working with twinned crystals, EPR is a powerful and sensitive technique to further our understanding of the rich and complex magnetic behavior of the planar CuO_2 materials.

ACKNOWLEDGMENTS

We wish to thank Professor D. R. Fredkin and H. Shore for helpful conversations. This research was partially supported at San Diego State University by the Natural Science Foundation (NSF) under Grant Nos. NSF-DMR-9117212 and NSF-INT-9202813, at Los Alamos National Laboratory was performed under the auspices of the United States Department of Energy and at the University of California San Diego by Grant Nos. NSF-DMR-89-15815 and AFOSR-90-0365, DE-AC04-76DP00789.

*Permanent address: Instituto de Fisica, UNICAMP, C.P. 6165, 13081 Campinas (SP), Brazil.

[1]Y. Kitaoka, K. Ishida, S. Hiramatsu, and K. Asayama, J. Phys. Soc. Jpn. **57**, 734 (1988); I. Watanabe, K. Kumagi, Y. Nakamura, T. Kimura, Y. Nakamichi, and H. Nakajima, *ibid.* **56**, 3028 (1987); D. Vaknin, S. K. Sinha, D. E. Moncton, D. C. Johnston, J. M. Newsam, C. R. Safinya, and H. E. King, Jr., Phys. Rev. Lett. **58**, 2802 (1987); Y. J. Uemura, W. J. Kossler, X. H. Yu, J. R. Kempton, H. E. Schone, D. Opie, C. E. Stronach, D. C. Johnston, M. S. Alvarez, and D. P. Goshorn, *ibid.* **59**, 1045 (1987); J. I. Budnick, B. Chamberland, D. P. Yang, Ch. Niedermayer, A. Golnik, E. Recknagel, M. Rossmanith, and A. Weidiner, Europhys. Lett. **5**, 651 (1988); J. I. Budnick, A. Golnik, Ch. Niedermayer, E. Recknagel, M. Rossmanith, A. Weidinger, B. Chamberland, M. Filipkowski, and D. P. Yang, Phys. Lett. A **124**, 103 (1987).

[2]P. W. Anderson, Science **235**, 1196 (1987); P. W. Anderson, G. Baskaran, Z. Zou, and T. Hsu, Phys. Rev. Lett. **58**, 2790 (1987); V. I. Emery, *ibid.* **58**, 2794 (1987); M. Cyrot, Solid State Commun. **62**, 821 (1987); J. R. Schrieffer, X.-G. Wen, and S-C. Zhang, Phys. Rev. Lett. **60**, 944 (1988); A. Aharony, R. J. Birgeneau, A. Coniglio, M. A. Kastner, and H. E. Stanley, *ibid.* **60**, 1330 (1988); R. J. Birgeneau, M. A. Kastner, and A. Aharony, Z. Phys. B **71**, 57 (1988).

[3]S. Oseroff *et al.*, Phys. Rev. B **41**, 1934 (1990).

[4]K. Yamada *et al.*, Phys. Rev. B **40**, 4557 (1989).

[5]Y. J. Uemura *et al.*, Phys. Rev. Lett. **59**, 1045 (1987); A. Weidinger *et al.*, *ibid.* **62**, 102 (1989).

[6]Y. Kitaoka *et al.*, Physica C **153-155**, 733 (1988); Y. Kitaoka *et al.*, J. Phys. Soc. Jpn. **56**, 3024 (1987); H. Nishihara *et al.*, *ibid.* **56**, 4559 (1989); I. Watanabe *et al.*, *ibid.* **59**, 1932 (1990).

[7]K. B. Lyons *et al.*, Phys. Rev. B **37**, 2353 (1988).

[8]R. D. Zysler *et al.*, Phys. Rev. B **44**, 9467 (1991).

[9]C. Chaillout *et al.*, Physica C **170**, 87 (1990); P. C. Hammell *et al.*, Phys. Rev. B **42**, 6781 (1990); K. Ueda *et al.*, Solid State Commun. **73**, 49 (1990).

[10]V. B. Kravchenko *et al.*, Fiz. Tverd. Tela (Leningrad) **11**, 3455 (1969) [Sov. Phys. Solid State **11**, 2898 (1970)]; L. Kratena *et al.*, Phys. Status Solidi **28**, 175 (1968).

[11]S. Oseroff *et al.* (unpublished).